Deposition of carbon nanotubes in the human respiratory tract: a theoretical approach

Robert Sturm

Department of Chemistry and Physics of Materials, University of Salzburg, Salzburg, Austria
Correspondence to: Dr. Robert Sturm. Brunnleitenweg 41, 5061 Elsbethen, Austria. Email: sturm_rob@hotmail.com.

Background: The study aims to describe the behavior of single-wall and multi-wall carbon nanotubes (SWCNT, MWCNT) in the human respiratory tract (HRT). Based on a theoretical deposition model, possible accumulation of these particles in different lung regions is subject to a detailed investigation. Predictions made by the theoretical approach should help to develop appropriate risk assessments for highly anisometric ultrafine particles.

Methods: Particle geometry expressed by the aspect ratio was approximated by using the aerodynamic diameter concept. Transport and deposition of SWCNT and MWCNT in the HRT was simulated with the help of a random-walk model based on the Monte-Carlo method. Random particle paths were computed for a stochastic lung architecture. For the simulation of particle deposition, empirical and analytical equations describing the physical processes exerting on the particles (i.e., Brownian motion, impaction, interception, and gravitational settling) were used. Simulations were conducted for adult lungs and two different breathing conditions.

Results: For sitting breathing (low tidal volume and breathing frequency), SWCNT exhibit a total deposition of 77.7%, with 34.3% being accumulated in the extrathoracic airways, 35.1% being deposited in the thoracic airways (lung generation 1–27), and 8.3% being targeted to the alveoli. MWCNT show a total deposition of 23.1%, whereby extrathoracic deposition amounts to 10.2%, bronchial deposition to 10.1, and alveolar deposition to 2.8%. For heavy-work breathing (high tidal volume and breathing frequency), total deposition of SWCNT is decreased (67.2%) and regional deposition is significantly modified (extrathoracic: 4.5%, bronchial: 43.5%, alveolar: 19.2%). Total deposition of MWCNT is reduced (15.4%), resulting in a remarkable change of extrathoracic (1.1%), bronchial (8.1%), and alveolar deposition (6.2%).

Conclusions: Inhalation of SWCNT and MWCNT may bear considerable health risks, as high numbers of inspired particles are deposited in lung regions (distal bronchioles, alveoli) being predisposed to various pulmonary diseases.

Keywords: Carbon nanotubes (CNT); human respiratory tract (HRT); deposition; aspect ratio; aerodynamic diameter; lung disease

Introduction

During the past decade, carbon nanotubes (CNT) have attracted high interest because of their extraordinary mechanical, electrical, and magnetic properties. CNT may be subdivided into single-wall carbon nanotubes (SWCNT), which consist of a single sheet of graphite rolled up to a seamless cylinder, and multi-wall carbon nanotubes (MWCNT), which include numerous telescoped SWCNT (1,2). SWCNT (density: 1.3–1.4 g·cm⁻³) have a diameter of several nanometers, but range in length up to several microns, whereas MWCNT (density: 1.8 g·cm⁻³) may reach diameters up to 100 nm and lengths up to 10 µm (3). From an aerodynamic point of view, SWCNT

may be regarded as ultrafine particles (<100 nm), whilst transport and deposition behavior of MWCNT may be most likely compared with that of asbestos fibers (4).

Although CNT have been evaluated as superior construction materials on microscopic level, potential hazards with regards to their inhalation have increasingly come into the focus of medical research (5-8). Experimental studies in rats using carbon-containing particulates yielded evidence that this particulate matter induces remarkable lung toxicity in the laboratory animals (7,8). Additionally, it could be demonstrated that the extent of toxicity negatively correlates with particle size and, on the other hand, exhibits a valuable enhancement with increasing particle surface area (9-11). Toxicological information on carbon fibers and on graphite particles is still rather sparse, although the number of respective studies has noticeably increased during the past decade (12-14). Epidemiological investigations, which mainly concentrated on graphite-containing dusts, could show an increased incidence of pneumoconiosis among workers that were exposed to such airborne particles. Health effects resulting from the exposure to CNT have only been described theoretically hitherto, thereby assuming a particle behavior very similar to that of insoluble asbestos or man-made vitreous fibers (MMVF) (2,4). According to several exposure assessment studies conducted at the beginning of the last decade, CNT have been classified as particles with low exposure levels at the workplace (15,16). More current CNT experiments in rats indicated a long-term storage of inhaled particle fractions in subepithelial tissues and, as a consequence of that, the induction of specific inflammatory processes (17,18). These results, however, propose a possible toxicity of SWCNT and MWCNT, which could also occur in human subjects exposed to these particulates.

Since CNT inhalation experiments with human probands are not practicable due to a high number of ethical reasons, theoretical particle transport and deposition models may contribute to extend our knowledge with regard to the behavior of such particulates in the human respiratory tract (HRT). In the meantime, accuracy of theoretical deposition predictions has continuously increased, because, first, deterministic lung architecture used in earlier models (19,20) has been replaced by a more realistic stochastic lung structure (21,22). Second, mathematical formulations of those deposition mechanisms exerting on inhaled particulates have been successively refined with the help of numerical approaches (23-25). Third, specific effects of ultrafine and non-spherical aerosol particles have found their increased consideration in modern computer

simulations (17,26,27). However, theoretical predictions concerning the pulmonary transport and deposition of CNT are characterized by remarkable paucity hitherto. Although few deposition data of CNT are already available (1-3,7), detailed deposition scenarios including different breathing conditions have to be additionally provided in order to obtain an advanced understanding of this particulate type.

The objective of this contribution is two-fold: first, the theoretical model for simulating transport and deposition physics of CNT in the HRT is subjected to a detailed description. Second, deposition scenarios for both SWCNT and MWCNT are outlined, thereby also discussing possible discrepancies with respect to the deposition of other particle types. Deposition predictions of both CNT categories are provided for breathing conditions indicating (I) the physical state of rest (sitting inhalation) and (II) the physical state of heavy exercise.

Methods

Modeling CNT geometry

Cylindrical geometry of CNT with its extreme aspect ratio (up to 1,000) was approximated by computation of dynamic shape factors, particle mobilities, and, as a result of these two parameters, the aerodynamic diameters. Generally, CNT, which have to be partly classified as ultrafine particles (see above), are transported within the so-called free-molecular regime, where the molecules of the gaseous transport medium are assumed to behave as particulates interacting with the nanotubes by a rapid sequence of collisions. Hence, the gas molecules exert a significant drag force on the nanotubes, which has to be considered as an essential contribution to the deposition of the particles in the HRT (see below). The free-molecular regime is further characterized by the circumstance that the relative velocity of the gas molecules at the surface of the particles is non-zero (28), so that the drag force emanating from the surrounding gas is again reduced by a certain factor. This so-called Cunningham slip correction factor mainly depends upon particle size, the mean free path of the gas molecules, and the temperature of the transport medium (29,30).

As found by experimental investigations (31,32), non-spherical particles are marked by an increased drag compared to spherical particles of similar size. This physical phenomenon is accounted for by definition of the dynamic shape factor (33). The correction factor describes the ratio
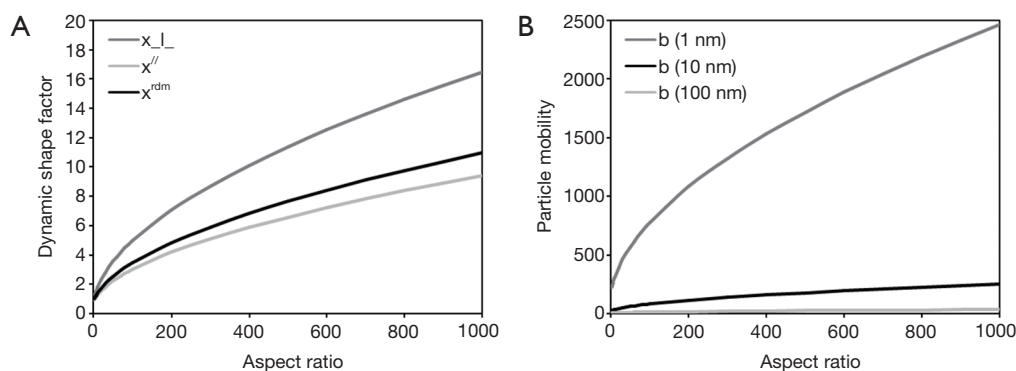
Figure 1 Important particle parameters used for modeling. (A) Dynamic shape factors (χ) for nanotubes with aspect ratios ranging from 3 to 1,000; (B) particle mobilities for nanotubes with different aspect ratios and three different cylindrical diameters (1 nm, 10 nm, and 100 nm).
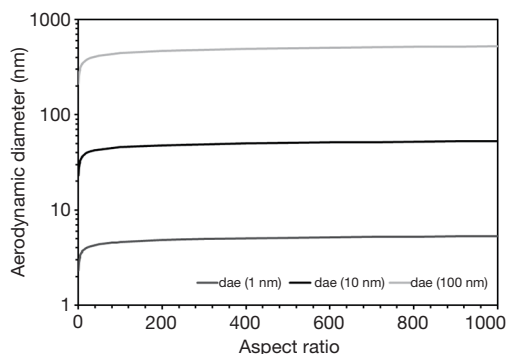

Figure 2 Aerodynamic diameter for nanotubes with different aspect ratios and three different cylindrical diameters (1 nm, 10 nm, and 100 nm).

of the drag force exerting on the non-spherical particle to the drag force exerting on a spherical particle with identical volume. The dynamic shape factor of non-spherical particles is commonly greater than 1 and increases its value with both increasing and decreasing aspect ratio (*Figure 1A*). In extreme cases (explosion dusts, aggregates with highly irregular shape), it may adopt values greater than 10 (34,35). Computation of the dynamic shape factor is additionally influenced by the orientation of the particle relative to the flow direction of the transport medium. This circumstance, however, is expressed by definition of specific dynamic shape factors for particles with perpendicular, parallel, and random orientation with respect to the gas stream (*Figure 1A*) (33-36). Particle mobilities are to be understood as an extension of the dynamic shape factors insofar as they also include the Cunningham slip correction factors noted above and thus provide additional information on particle

size (*Figure 1B*).

The aerodynamic diameter, corresponding to the diameter of a unit-density sphere with exactly the same aerodynamic behavior as the particle of interest, includes the factors described above as well as an additional parameter known as the so-called volume-equivalent diameter (17,26,27-29,33-36). This represents the diameter of a sphere with identical density and volume as the studied particle. Since the aerodynamic diameter positively correlates with the volume-equivalent diameter, any increase of the aspect ratio also results in a respective enhancement of the aerodynamic diameter (*Figure 2*). As an interesting side-effect, increase of the aerodynamic diameter may be evaluated as significant for aspect ratios ranging from 3 to 50, whereas any further increase of the length/diameter ratio has less spectacular effects on the aerodynamic diameter. The aerodynamic diameter, however, is used for the theoretical investigation of CNT transport and deposition in the HRT (1-4).

Mathematical approach to CNT transport and deposition in the human lungs

For an appropriate simulation of CNT behavior in the HRT, the FORTRAN computer program IDEAL 6 (Inhalation, Deposition, and Exhalation of Aerosol in/from the Lungs) originally proposed by Koblinger and Hofmann (19) and further improved by numerous co-workers (17,26,27,37-41) was used. The program is based on a stochastic structure of the HRT, where airway tubes of a given lung generation are characterized by noticeable variations with regard to their geometric properties. Theoretical construction of this close-to-reality lung geometry is made possible by generation-
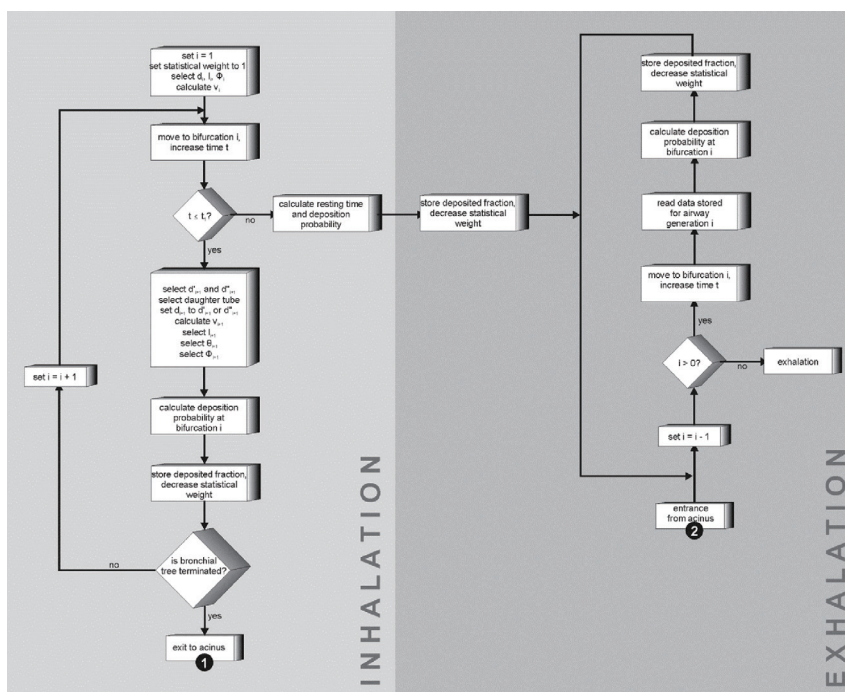
Figure 3 Flow chart illustrating the mathematical algorithm that stands behind the computation of CNT transport and deposition in the bronchial airways (19). CNT, carbon nanotubes.

specific probability density functions for airway diameters, airway lengths, bifurcation angles, and gravity angles (i.e., the angles of the airways relative to the vertical direction), which were determined from morphometric data sets of the tracheobronchial tree (42) and the acinar region (43). For each airway, the respective geometric information is selected from these probability density functions by application of the random number concept. The decision of the program to construct an alveolated bronchiolus (bronchiolus respiratory) or not is founded on (I) the size of the airway, with a diameter <0.33 mm resulting in the consideration of alveoli, and (II) the airway generation, with alveolated tubes occurring at least in the 13th lung generation. Alveoli themselves are assumed to adopt spherical geometry with a uniform diameter of 250 µm and a circular orifice having 65% of the diameter of the median alveolar circle (19).

Particles inhaled from the ambient air follow random pathways in the lung. By using the Monte Carlo concept, large numbers (e.g., 10,000) of such random particle walks may be generated (19). Particle transport is continued until (I) the particle is deposited, (II) the particle enters an alveolus, or (III) the time assumed for inhalation has expired. Additional improvement of the Monte Carlo statistics is provided by application of the statistical weight

technique, according to which each particle entering the tracheobronchial tree adopts a unit weight. At each bifurcation, this unit weight is multiplied by (1 – p), with p denoting the deposition probability within the bifurcation unit. The final fraction of deposited particles is computed by producing the product to the actual weight, the related deposition probability, and the number of particles considered for the simulation procedure. In the acinar lung region, the statistical weight method is not applied. If the particle enters an alveolus, it is supposed to be affected by the mixing process between tidal and residual air with a probability of 25%, whereas non-mixing of respective air volumes and behavior of the particle according to the first-in-last-out approximation is assumed to adopt a probability of 75% (19). Based on this hypothesis a related deposition probability is calculated. If the particle has neither deposited nor entered an alveolus and inhalation time has finished, its transport along the random path is stopped, and deposition probability during breath-hold time is computed. If no deposition scenario could be determined during this time span, the particle is exhaled by following the random path back to the extrathoracic region. Deposition mechanisms exerting on the particle during expiration are the same as those exerting on the particle during inhalation (*Figures 3,4*).
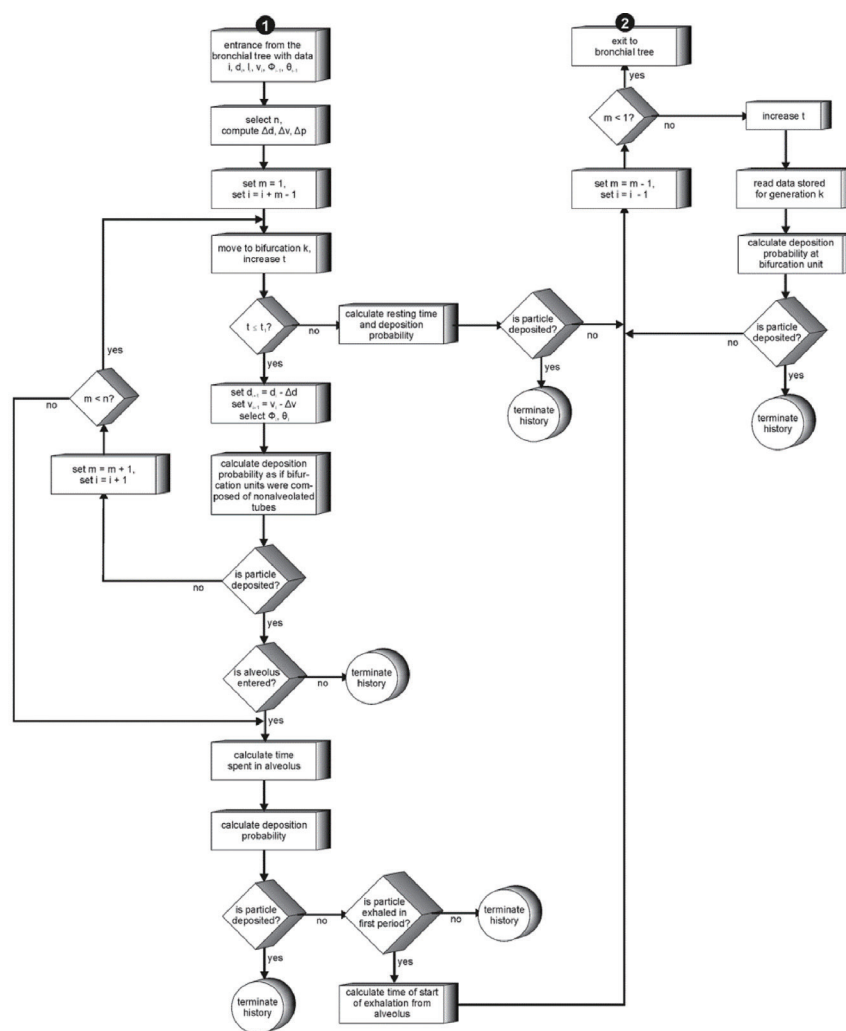
Figure 4 Flow chart illustrating the mathematical algorithm that stands behind the computation of CNT transport and deposition in the acinar region (19). CNT, carbon nanotubes.

Results

Regional deposition of CNT

Model predictions for regional CNT deposition were conducted by assuming intermediately sized SWCNT (diameter: 7 nm, length: 700 nm) and MWCNT (diameter: 70 nm, length: 7 µm) as well as breathing through the mouth (*Table 1*). Regarding the uptake of CNT through the oral pathway of the respiratory tract, results summarized in Tab. 1 include several interesting aspects. Under sitting breathing condition, SWCNT are preferably deposited in the airways of the head (34.3%), followed by the bronchial (24.6%) and bronchiolar (10.5%) airways. The alveoli, however, represent the preferential deposition target for 8.3% of the inhaled particles. The fraction of exhaled particles amounts to 22.3%. A completely different situation is given for MWCNT, which are deposited in the extrathoracic region by 10.2%, in the bronchi by 5.8%, in the bronchioles by 4.3%, and in the alveoli by 2.8%. Here, the exhaled particle fraction adopts a value of 77.9%. By carrying out heavy exercise during the breathing process, several characteristics of SWCNT and MWCNT become remarkably changed (*Table 1*). SWCNT are mostly deposited in the bronchioles (24.1%), followed by the bronchi (19.4%) and alveoli (19.2%), whereas the extrathoracic compartment represent the deposition target for 4.5% of the particles. MWCNT, on the other hand, show enhanced deposition in the bronchioles (5.3%) and

Table 1 CNT deposition in different regions of the human respiratory tract after assumption of mouth breathing

Physical condition	Region	Deposition SWCNT (%)	Deposition MWCNT (%)
Sitting breathing	Head	34.3	10.2
	Bronchi	24.6	5.8
	Bronchioli	10.5	4.3
	Alveoli	8.3	2.8
Heavy exercise	Head	4.5	1.1
	Bronchi	19.4	2.8
	Bronchioli	24.1	5.3
	Alveoli	19.2	6.2

CNT, carbon nanotubes; SWCNT, single-wall carbon nanotubes; MWCNT, multi-wall carbon nanotubes.
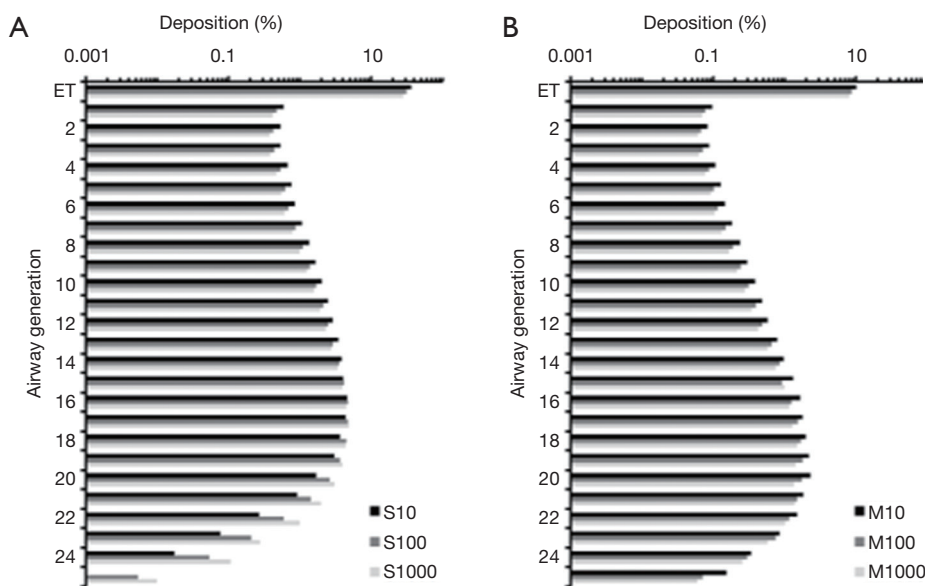

Figure 5 Generation-by-generation deposition of SWCNT (A) and MWCNT (B) with different aspect ratios (10, 100, and 1,000). Deposition patterns were computed for sitting breathing conditions and aerosol inhalation through the mouth. SWCNT, single-wall carbon nanotubes; MWCNT, multi-wall carbon nanotubes.

the alveoli (6.2%). Total deposition of SWCNT changes from 77.7% for sitting breathing to 67.2% for heavy-exercise breathing, whereas total deposition of MWCNT is modified from 23.1% (sitting breathing) to 15.4% (heavy-exercise breathing).

Generation-by-generation deposition of CNT

For the theoretical investigation of CNT deposition in the single airway generations of the human lungs SWCNT and MWCNT adopting aspect ratios of 10,100 and 1,000 were used, respectively. Therefore SWCNT with a uniform diameter of 7 nm measured 70,700 and 7,000 nm in length, whereas MWCNT (diameter: 70 nm) had lengths of 700, 7,000 and 70,000 nm. Results of deposition computations based on (I) sitting breathing and (II) heavy-work breathing are summarized in the graphs of *Figures 5,6*.

Under conditions of sitting breathing short SWCNT (S10) exhibits their maximal deposition in airway generation 16 (4.49%) and penetrate in valuable amounts to generation
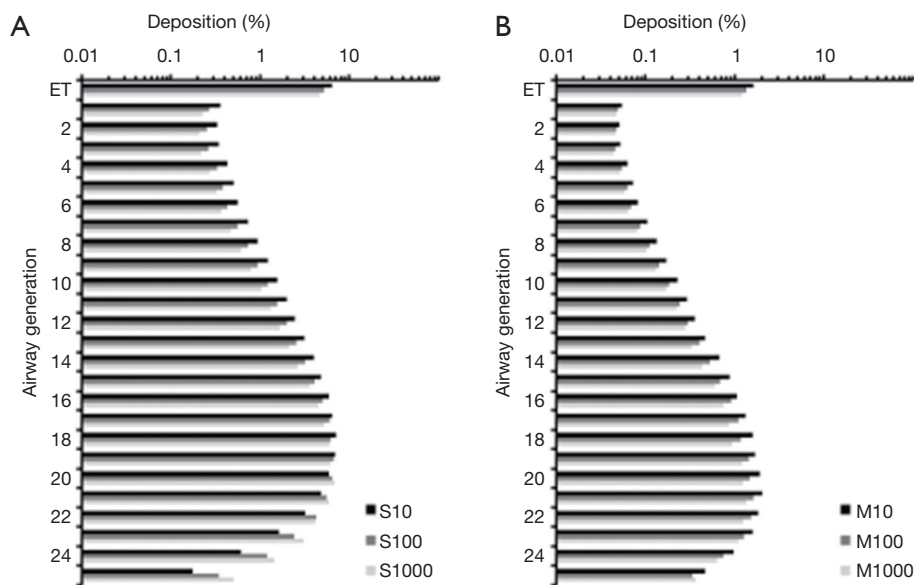
Figure 6 Generation-by-generation deposition of SWCNT (A) and MWCNT (B) with different aspect ratios (10, 100, and 1,000). Deposition patterns were computed for heavy-exercise breathing conditions and aerosol inhalation through the mouth. SWCNT, single-wall carbon nanotubes; MWCNT, multi-wall carbon nanotubes.

24. Longer nanotubes produce both higher deposition rates and a more pronounced lung penetration. Therefore intermediate SWCNT (S100) deposit in airway generation 16 by 4.65% and still show a valuable accumulation in generation 26. Long SWCNT (S1000) have their deposition maximum in airway generation 17 (4.78%) and also reach generation 26. In the case of MWCNT, airway-related deposition is generally reduced by about 60% to 80%, whereby any increase of the aspect ratio has a negative effect on particle accumulation. Concretely speaking, short MWCNT (M10) exhibit a deposition maximum in airway generation 20 (2.28%) and penetrate with remarkable amount to generation 27. Intermediate MWCNT (M100) preferably deposit in airway generation 19 (1.76%) and long MWCNT (M1000) show their preferential deposition in generation 18 (1.46%). Both particle classes penetrate towards generation 27.

Any switch from sitting breathing to heavy-work breathing has several effects on CNT deposition in single airways of the human lungs. Regarding SWCNT both generation-specific deposition rates and penetration distances of the particles are significantly increased. Therefore S10 exhibit their maximal deposition in generation 18 (7.05%) and reach generation 27, whereas S100 deposit by 6.63% in generation 19 (penetration towards generation 26) and S1000 deposit by 6.71% in

generation 20 (penetration towards generation 27). With regard to MWCNT generation-specific deposition is subject to a decrease, whereas penetration depth is further increased. All particle categories show their deposition maxima in airway generation 21 and deposit there by 2.02% (M10), 1.62% (M100) and 1.34% (M1000). Deposition reaches generation 27 (M10) or 28 (M100, M1000).

Discussion

Comparison of regional deposition values obtained for different classes of CNT and different breathing conditions bears several interesting aspects. First, SWCNT are commonly characterized by higher total and regional deposition than MWCNT; second, any enhancement of the inhalation flow rate, being the result of increasing physical strain, results either in a displacement of deposition towards more distal lung regions or a decrease of the deposited particle fraction and increase of the number of exhaled particles; and third, particles passing the nasal airways are filtered to a higher extent in the extrathoracic region than nanotubes being inhaled through the oral pathway. All these essential finds may be led back to the circumstance that aerodynamic diameters generated for SWCNT adopt values around 50 nm, whereas aerodynamic diameters computed for MWCNT are on the order of 500 nm. This difference of

one order of magnitude has partly aggravating consequences for particle behavior in the bronchial and alveolar structures. As outlined in numerous studies (17,21-28), main deposition mechanism exerting on nanoparticles is Brownian motion, whereby the efficiency of this physical deposition mechanism continuously declines within a particle size interval ranging from 1 nm (molecule size) to 100 nm [upper size limit for ultrafine particles (19,21)].

Whilst in the case of SWCNT continuous increase of the aspect ratio implies an enhancement of local deposition and penetration depth, rising length of MWCNT, on the other hand, produces a reverse effect. These theoretical findings, which greatly manifest under sitting breathing conditions, can be lead back to the fact that SWCNT adopt aerodynamic diameters ranging from 40 to 50 nm (*Figure 2*). This small particle size makes them highly susceptible to diffusive processes (1-4). Smaller (i.e., shorter) SWCNT are already filtered in the extrathoracic airways to a higher extent, so that lower amounts of particles can reach the small airways and alveoli. Larger SWCNT, on the other side, can more efficiently escape from the filtering process in the head and thus can be transported to the peripheral lungs in higher amounts. This phenomenon results in slightly higher deposition rates in the small bronchiolar and alveolar structures (1-4,12-18). It has to be noted in this context that the alignment of the nanotubes within the inhaled air stream can play a major role in so far as particles being oriented parallel to the stream lines have a much higher chance for reaching the closing sacs of the acinar region (16-18). MWCNT adopt aerodynamic diameters between 400 and 500 nm. These particles are characterized by a continuous attenuation of diffusive processes, but also largely escape from mass-related deposition mechanisms such as inertial impaction or gravitational settling (19-21). Hence, a permanent decrease of local deposition rates and penetration depths is observed, finally resulting in a higher fraction of exhaled particles.

Enhancement of the inhalation flow rate has a positive effect on the local deposition and lung penetration of SWCNT, but a negative effect on local deposition and penetration of MWCNT. Due to higher streaming velocities of the inspired air SWCNT have lower residence times in the extrathoracic airways, causing a diminution of deposition by diffusive processes at these sites and an increasing transport towards more peripheral lung sites (12-18). Since in the small airways air flow becomes laminar, those particles which have been escaped from extrathoracic and bronchial deposition are preferably accumulated at the walls

of the non-ciliated bronchiolar structures (38,39,44,45). In the case of MWCNT any increase of the streaming velocity also results in a further decline of deposition by Brownian motion and an enhancement of exhaled particle fractions.

Conclusions

Based on the theoretical results presented above deposition of SWCNT and MWCNT mainly depends on particle properties (diameters, lengths) as well as breathing conditions (tidal volume, breath-cycle time). Although MWCNT exhibit lower deposition rates than SWCNT, both classes of nanotubes are accumulated in the lung airways and alveoli in considerable amounts. By increasing the inhalation flow rate due to enhanced physical stress, nanotubes commonly tend to produce higher deposition rates in the peripheral regions of the lungs which represents an essential development from a medical point of view. Previous studies could demonstrate that CNT being characterized by extreme biopersistence have a similar effect on lung tissues and cells as asbestos fibers and thus have to be regarded as serious health hazards. It is assumed that these particles cause a significant remodelling of distal lung tissues and may be also responsible for the induction of malignant cell transformations. Concerning the last point, further studies have to be carried out in the near future.

Footnote

Conflicts of Interest: The author has completed the ICMJE uniform disclosure form (available at http://dx.doi.org/10.21037/jphe.2018.05.03). The author has no conflicts of interest to declare.

Ethical Statement: The author is accountable for all aspects of the work in ensuring that questions related to the accuracy or integrity of any part of the work are appropriately investigated and resolved.

Open Access Statement: This is an Open Access article distributed in accordance with the Creative Commons Attribution-NonCommercial-NoDerivs 4.0 International License (CC BY-NC-ND 4.0), which permits the non-commercial replication and distribution of the article with

References

1. Sturm R. Theoretical deposition of nanotubes in the respiratory tract of children and adults. Ann Transl Med 2014;2:6.
2. Sturm R. Nanotubes in the respiratory tract - Deposition modeling. Z med Phys 2015;25:135-45.
3. Sturm R. Inhaled nanoparticles. Phys Today 2016;69:70-1.
4. Sturm R. A stochastic model of carbon nanotube deposition in the airways and alveoli of the human respiratory tract. Inhal Toxicol 2016;28:49-60.
5. Maynard AD. Safe handling of nanotechnology. Nature 2006;444:267-9.
6. Donaldson K, Aitken R, Tran L, et al. Carbon nanotubes: a review of their properties in relation to pulmonary toxicology and workplace safety. Toxicol Sci 2006;92:5-22.
7. Högberg SM. Modeling nanofiber transport and deposition in human airways. Lulea: Tech Univ Lulea, 2010.
8. Warheit DB, Laurence BR, Reed KL, et al. Comparative pulmonary toxicity assessment of single-wall carbon nanotubes in rats. Toxicol Sci 2004;77:117-25.
9. Maynard AD. Nanotechnology: The next big thing, or much ado about nothing? Ann Occup Hyg 2007;51:1-12.
10. Poland CA, Duffin R, Kinloch I, et al. Carbon nanotubes introduced into the abdominal cavity of mice show asbestos-like pathogenicity in a pilot study. Nat Nanotechnol 2008;3:423-8.
11. Duffin R, Clouter A, Brown D, et al. The importance of surface area and specific reactivity in the acute pulmonary inflammatory response to particles. Ann Occup Hyg 2002;46:242-5.
12. Sturm R. Theoretical deposition of carcinogenic particle aggregates in the upper respiratory tract. Ann Transl Med 2013;1:25.
13. Sturm R. Spatial visualization of theoretical nanoparticle deposition in the human respiratory tract. Ann Transl Med 2015;3:326.
14. Sturm R. Deposition of ultrafine particles with various shapes in the human alveoli – a model approach. Comp Math Biol 2016;5:4.
15. Sturm R. A theoretical approach to the deposition of cancer-inducing asbestos fibers in the human respiratory tract. TOLCJ 2009;2:1-11.
16. Sturm R, Hofmann W. Modellrechnungen zur Deposition nicht-sphärischer Teilchen in den oberen Luftwegen der menschlichen Lunge. Z Med Phys 2009;19:38-46.
17. Sturm R. Theoretical models of carcinogenic particle deposition and clearance in children's lungs. J Thorac Dis 2012;4:368-76.
18. Sturm R, Hofmann W. A theoretical approach to the deposition and clearance of fibers with variable size in the human respiratory tract. J Hazard Mater 2009;170:210-8.
19. Koblinger L, Hofmann, W. Monte Carlo modeling of aerosol deposition in human lungs. Part I: Simulation of particle transport in a stochastic lung structure. J Aerosol Sci 1990;21:661-74.
20. Hofmann W, Sturm R, Winkler-Heil R, et al. Stochastic model of ultrafine particle deposition and clearance in the human respiratory tract. Radiat Prot Dosimetry 2003;105:77-80.
21. International Commission on Radiological Protection (ICRP). Human respiratory tract model for radiological protection, Publication 66. Oxford: Pergamon Press, 1994.
22. Asgharian B, Anjilvel S. The effect of fiber inertia on its orientation in a shear flow with application to lung dosimetry. Aerosol Sci Technol 1995;23:282-90.
23. Sturm R, Hofmann W. Stochastisches Modell zur räumlichen Visualisierung von Teilchendepositionsmustern in der Lunge und ihre Bedeutung in der Lungenmedizin. Z Med Phys 2006;16:140-7.
24. Sturm R. A computer model for the simulation of nonspherical particle dynamics in the human respiratory tract. Phys Res Int 2012:1-11.
25. Sturm R, Hofmann W. 3D-Visualization of particle deposition patterns in the human lung generated by Monte Carlo modeling: methodology and applications. Comput Biol Med 2005;35:41-56.
26. Sturm R. Theoretical and experimental approaches to the deposition and clearance of ultrafine carcinogens in the human respiratory tract. Thorac Cancer 2011;2:61-8.
27. Sturm R. A computer model for the simulation of fiber-cell interaction in the alveolar region of the respiratory tract. Comput Biol Med 2011;41:565-73.
28. Hinds WC. Aerosol Technology: Properties, Behavior, and Measurement of Airborne Particles. New York: John Wiley, 1999.
29. Dahneke B. Slip correction factors for nonspherical bodies–I Introduction and continuum flow. J Aerosol Sci 1973;4:139-45.
30. Dahneke B. Slip correction factors for nonspherical bodies–II Free molecular flow. J Aerosol Sci 1973;4:147-61.

31. Willeke K, Baron PA. Aerosol measurement. New York, NY: John Wiley, 1993.
32. DeCarlo PF, Slowik JG, Worsnop DR, et al. Particle morphology and density characterization by combined mobility and aerodynamic diameter measurements. Aerosol Sci Technol 2004;38:1185-205.
33. Fuchs NA. The Mechanics of Aerosols. New York: Pergamon Press, 1964.
34. Kasper G. Dynamics and measurement of smokes. I Size characterization of nonspherical particles. Aerosol SciTechnol 1982;1:187-99.
35. Sturm R. Theoretical models for dynamic shape factors and lung deposition of small particle aggregates originating from combustion processes. Z med Phys 2010;20:226-34.
36. Su WC, Cheng YS. Deposition of fiber in a human airway replica. J Aerosol Sci 2006;37:1429-41.
37. Hofmann W, Bolt L, Sturm R, et al. Simulation of three-dimensional particle deposition patterns in human lungs and comparison with experimental SPECT data. Aerosol Sci Technol 2005;39:771-81.
38. Sturm R, Hofmann W. A computer program for the simulation of fiber deposition in the human respiratory tract. Comput Biol Med 2006;36:1252-67.
39. Sturm R. Theoretical approach to the hit probability of lung-cancer-sensitive epithelial cells by mineral fibers with various aspect ratios. Thoracic Cancer 2010;1:116-25.
40. Sturm R. A three-dimensional model of tracheobronchial particle distribution during mucociliary clearance in the human respiratory tract. Z med Phys 2013;23:111-9.
41. Sturm R. Computer-aided generation and lung deposition modeling of nano-scale particle aggregates. Inhal Toxicol 2017;29:160-8.
42. Raabe OG, Yeh HC, Schum GM et al. Tracheobronchial geometry: Human, dog, rat, hamster – A compilation of selected data from the project respiratory tract deposition models. Report LF-53. Albuquerque, AZ: Lovelace Foundation, 1976.
43. Haefeli-Bleuer B, Weibel ER. Morphology of the human pulmonary acinus. Anat Rec 1988;220:401-14.
44. Sturm R. Modeling the deposition of bioaerosols with variable size and shape in the human respiratory tract–A review. J Adv Res 2012;3:295-304.
45. Sturm R. Inhalation of nanoplatelets–theoretical deposition simulations. Z med Phys 2017;27:274-84.